Optimization of computer-generated holograms for dynamic optical manipulation with uniform structured light spots

Jing Bu (步 敬)[1], Guanghui Yuan (苑光辉)[2], Yuyang Sun (孙宇扬)[2], Siwei Zhu (朱思伟)[3], and Xiaocong Yuan (袁小聪)[1*]

[1]*Institute of Modern Optics, Key Laboratory of Optoelectronic Information Science and Technology, Ministry of Education of China, Nankai University, Tianjin 300071, China*

[2]*School of Electrical and Electronic Engineering, Nanyang Technological University, Nanyang Avenue 639798, Singapore*

[3]*Nankai University Affiliated Hospital, Tianjin 300121, China*

[*]*Corresponding author: xcyuan@nankai.edu.cn*

Received October 8, 2010; accepted January 28, 2011; posted online May 6, 2011

An optimized iterative technique combining the merits of conventional Gerchber-Saxton (G-S) and adaptive-additive (A-A) algorithms to design multilevel computer-generated holograms for the creation of a desirable structured intensity pattern for multiple optical manipulation is theoretically adopted. Optical trap arrays are demonstrated with the help of liquid crystal spatial light modulator and a microscopic optical tweezer system. Additionally, continuous locked-in transport and deflection of microparticles with the generated optical lattice is proven experimentally. The proposed method possesses apparent high efficiency, high uniformity, and dynamic and reconfigurable advantages.

OCIS codes: 120.4610, 350.4855.
doi: 10.3788/COL201109.061202.

Optical tweezers have been proven to be capable of manipulating and sorting high resolution objects with noninvasive feature whose sizes range from nanometers to micrometers[1]. These tweezers showed widespread applications in physics and biochemistry, for example studies of orbital angular momentum with optical vortices[2,3], optical actuator[4], optical tweezers[5,6], and laser guidance[7]. Unlike traditional approaches which use fluorescence markers for sorting[8], the all-optical sorting method relies on the intrinsic physical attributes of particles, such as geometrical size and refractive index as labels for sorting. Hence, it is a continuous, noninteractive, and minimally invasive method.

Several approaches for generating optical lattice patterns for sorting applications, including multibeam interference[9], holographic diffractive elements[10], generalized phase contrast[11], microlens array[12], etc., have been reported. We adopt computer-generated holograms (CGHs) to create structured optical pattern with iterative optimization designs. The light-spot uniformity will not be influenced by the poor uniformity of input beam. The fabrication of binary CGH is compatible with general microlithography technique. In addition, the CGHs realized with spatial light modulator (SLM) have the ability to create a dynamic optical pattern. Based on these advantages, the CGHs are applied to the dynamic multiple optical trapping and continuous locked-in transport of microparticles.

The design of CGH is based on Gerchber-Saxton (G-S) algorithm which belongs to the group of iterative Fourier transformation algorithms (IFTAs)[13,14]. Its flowchart is shown in Fig. 1. A is the amplitude of illuminating beam and a random initial phase φ_0 is chosen. The complex amplitude of incident beam is transformed integrally through fast Fourier transformation (FFT) into an image with $E_{\rm out}(k) = A_{\rm out}(k)\exp[{\rm i}\varphi_{\rm out}(k)]$, where k is the number of iterations. Subsequently, the intensity-intensity constraint is exerted on this computed image to form new complex amplitude $\overline{E_{\rm out}}(k)$,

$$\overline{E_{\rm out}}(k) = A_{\rm obj}\exp[{\rm i}\varphi_{\rm out}(k)], \tag{1}$$

where $A_{\rm obj} > 0$ is the desirable amplitude in image plane. This new complex amplitude $\overline{E_{\rm out}}(k)$ is transformed inversely to $\overline{E_{\rm in}}(k) = \overline{A_{\rm out}}\exp(\overline{{\rm i}\varphi_{\rm in}}(k))$. Finally, $\overline{\varphi_{\rm in}}(k)$ is quantized and used as the phase of $E_{\rm in}(k)$ in a new iteration. The quantization is described by,

$$\begin{aligned}&\varphi \in [0, 2\pi),\\ &\varphi_{\rm q} = {\rm floor}[\varphi \times {\rm level}/(2\pi)] \times 2\pi/{\rm level}.\end{aligned} \tag{2}$$

The iteration is repeated until the root mean square error (RMSE) reaches a predefined value. When all of the iterations are over, the computed phase-only hologram has $\varphi_{\rm in} = \varphi_{\rm in}(k)$. The RMSE is a parameter describing the closeness of the computed reconstruction image to the object reconstruction image. It is usually defined as

$${\rm RMSE} = \int_{-\infty}^{\infty}\int |A_{\rm out}(\xi,\eta) - A_{\rm obj}(\xi,\eta)|^2 {\rm d}\xi{\rm d}\eta. \tag{3}$$

Generally, the G-S algorithm begins with an initial estimate of phase distribution, which can be random. The initial phase element is mapped to the observation plane according to a certain propagation rule. The function in the observation plane is imposed on some constraints as required and the modified function is reversely mapped to the diffractive optical element (DOE) plane. In this step, the transmittance function of DOE is usually in a complex form. However, the amplitude information is abandoned and the phase-only function goes through the mapping again. This time, the mapped field is evaluated by considering several criteria. If the change of

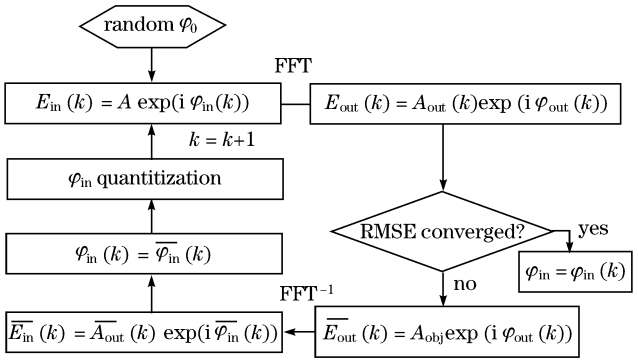

Fig. 1. Flowchart of the G-S algorithm.

performance is regarded as large, then the process will continue. Otherwise, it will be terminated and the previous phase function is pulled out as the optimized phase function.

A two-dimensional (2D) CGH was designed to generate a 5×5 array of optical spots with uniform intensity based on the G-S phase retrieval algorithm. The CGH was assumed to be illuminated by a plane wave, and the profile of incident light beam was sampled with 256×256 pixels. Usually, the IFTA algorithm will converge after approximately 20 iterations. In this study, 50 iterations were run to ensure a relative low RMSE. In Fig. 2, the RMSEs of the G-S algorithm decrease rapidly in several of the initial iterations. However, no significant reduction in the following iterations is observed. The final RMSEs are 0.1345, 0.1133, 0.1042, and 0.0962 after 10, 20, 30, and 50 iterations, respectively. Moreover, the diffraction efficiency of computed phase hologram is 0.9804 after 50 iterations. Figure 3 shows the computed 2D and one-dimensional (1D) intensity distributions of a 5×5 spot array in the frequency plane at $k = 50$. The 1D result was extracted from the corresponding 2D result to illustrate the uniformity of object pattern at certain iterations.

The convergence of G-S algorithm features a stagnation effect similar to general observation. To increase the convergence rate, modifications to the algorithm are introduced. One of the modified G-S algorithms is the adaptive-additive (A-A) algorithm. It should be noted that there is only a small difference between A-A and G-S algorithms. The amplitude $A_{out}(k)$ of the kth iteration step in G-S algorithm (highlighted in Fig. 1) is replaced by the desirable amplitude A_{obj} to form a new complex amplitude $\overline{E_{out}}(k)$:

$$\overline{E_{out}}(k) = \begin{cases} [\alpha A_{obj} + (1-\alpha) A_{out}(k)] \exp[i\varphi_{out}(k)], \\ \quad A_{obj} > 0 \\ A_{out}(k), \quad \text{else} \end{cases}, \tag{4}$$

where α is a coefficient to be chosen. This means that the amplitude $A_{out}(k)$ of Fourier transform is totally removed in the G-S algorithm. However, in each iteration of A-A algorithm, the $A_{out}(k)$ will not be directly replaced with A_{obj} after the FFT of initial complex input complex amplitude, but with a linear combination with different weights of A_{obj} and $A_{out}(k)$.

Using the same parameters as those of G-S algorithm, a new phase-only hologram with 128 phase levels is computed through modified A-A algorithm ($\alpha = 1$). According to Fig. 4, the RMSE of A-A algorithm does not decrease as rapidly as that of G-S in the first several iterations. However, the stagnation problem of G-S is partly overcome. The final RMSEs are 0.1455, 0.1055, 0.0864, and 0.0663 after 10, 20, 30, and 50 iterations, respectively. The diffraction efficiency of computed phase hologram is 0.8766 after 50 iterations. Figure 5 provides the computed 2D and 1D intensity distribution in the frequency plane at $k = 50$.

The A-A algorithm partly solved the converging stagnation problem of G-S algorithm and reduced the RMSE. However, two disadvantages were shown. Firstly, the convergence rate obviously slowed down at several initial iterations, so that more iterations were required by the A-A algorithm to realize a desirable RMSE. Secondly, the diffraction efficiency of A-A algorithm was reduced to 0.8766, which was approximately 10% smaller than

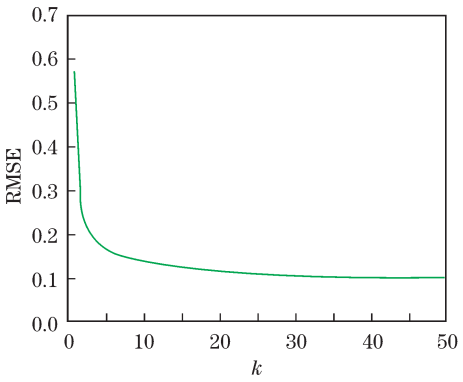

Fig. 2. RMSE versus iteration times k of the G-S algorithm.

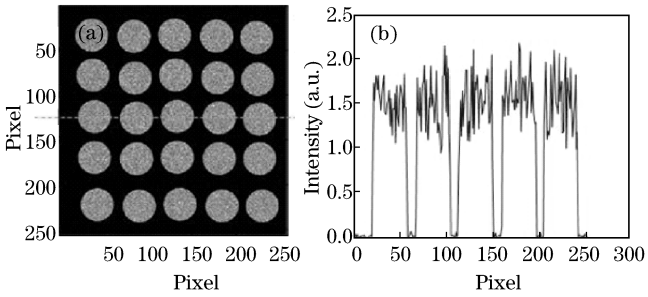

Fig. 3. Simulation results of (a) 2D and (b) 1D intensity distributions of 5×5 spot array with G-S after 50 iterations.

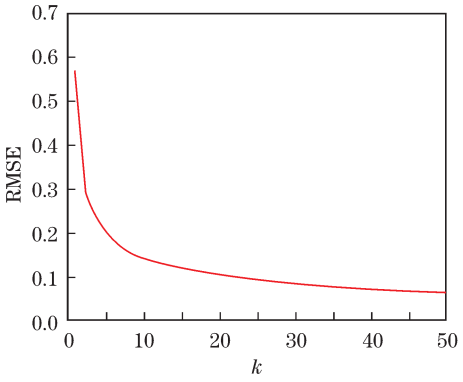

Fig. 4. RMSE versus iteration times k of the A-A algorithm ($\alpha = 1$).

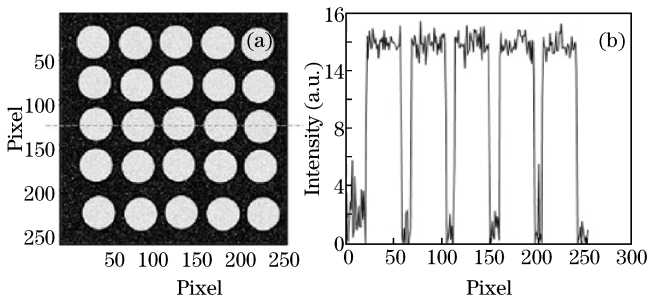

Fig. 5. Simulation results of (a) 2D and (b) 1D intensity distributions of 5×5 spot array with A-A algorithm after 50 iterations.

that of G-S algorithm. In this case, we adopted a third algorithm, GS-AA, which combined the merits of both G-S and A-A algorithms for CGH design. In the flow of the GS-AA algorithm, the first 10 iterations are implemented following the GS algorithm with the replacement of Eq. (1), while the remaining 40 iterations are implemented with the replacement of Eq. (4) used in the A-A algorithm. Consequently, the RMSE of GS-AA algorithm drops at the same speed as that of G-S algorithm and no further stagnation in the remaining iterations is observed. The RMSEs are 0.1348, 0.0529, 0.0454, and 0.0431 after 10, 20, 30, and 50 iterations, respectively. Furthermore, the diffraction efficiency of GS-AA reaches 0.9224, which is a compromise value between the G-S and A-A algorithms.

Optical system based on the optimized phase hologram and SLM for multiple trapping is shown in Fig. 6. SLM is introduced to realize a maximum phase step with reconfigurable and dynamic control ability advantages. This provides the difference from other time-consuming microfabrication techniques such as laser writing, electron beam writing, and gray-scale lithography. We used the programmable phase modulator (PPM) produced by Hamamatsu. It is an electrically addressed phase modulator which uses an optically addressed, parallel aligned nematic liquid crystal SLM. This is efficiently coupled with an electrical signal input-type liquid crystal display (LCD) through lens and incorporates a write-in laser diode (LD) module. The PPM X8267 series uses a LCD to simplify the computer control problems and adopts an optical system to eliminate the unwanted diffraction light originating from the LCD pixel structure. Furthermore, PPM offers large phase modulation. In the phase range between 0 and 2π, PPM is capable of providing as many as approximately 200 levels, making it competitive and attractive in realizing DOEs. The laser source was the Laser Quantum MPC 6000 (Ventus) at 532 nm with an output power up to 1.5 W, the output beam of which was linearly polarized. The laser beam with a diameter of approximately 2 mm was collimated and expanded four times by a telescope system composed of two converging lenses to fit the active areas of the SLM. The half-wave plate within the optical path was used to change the direction of linear polarization to match the phase mode of SLM. The SLM was utilized as a reflective mode without employing a beam splitter to avoid high loss of light energy. The CGH was displayed on the screen of a computer and transmitted to the SLM. Hence, once the collimated beam incident on the SLM with a small angle is achieved, the designed optical intensity pattern will be formed at the back focal plane of subsequent converging lenses. If a video is played on the screen of a computer, a dynamic optical pattern is displayed at the designed plane as well. After the grating, the two converging lenses constituted a telescope system which enabled the plane of the SLM to conjugate to the plane of the back aperture of the objective. The aperture was adopted to stop the unnecessary diffraction order. Hence, the second lens converged the light beam into the aperture of the objective and subsequently focused on the desirable optical trap array on the sample plane. The oil immersion objective lens (100×, Carl-Zeiss) was mounted on the upright microscope (Axiostar, Carl-Zeiss). The motion of the particles was captured by a charge-coupled device (CCD) camera and displayed on the screen of monitor. A dichroic mirror was adopted to reflect the laser beam to permit the beam to enter the aperture of objective lens while allowing the illumination light and the image of the trapping of particles to pass through a CCD camera connected to a computer, where the particle motions were observed in real time.

We design a video composed of two holograms to demonstrate the dynamic multiple optical trapping ability of the SLM system. The two desirable object patterns are shown in Fig. 7(a). The design of CGH is based on the hybrid GS-AA algorithm, in which the profile of incident light beam is sampled with 256×256 pixels and the number of phase levels is 128. The two CGHs

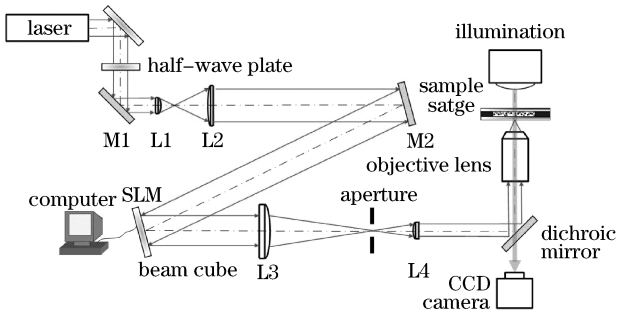

Fig. 6. Optical system based on SLM for multiple trapping. L: lens; M: mirror.

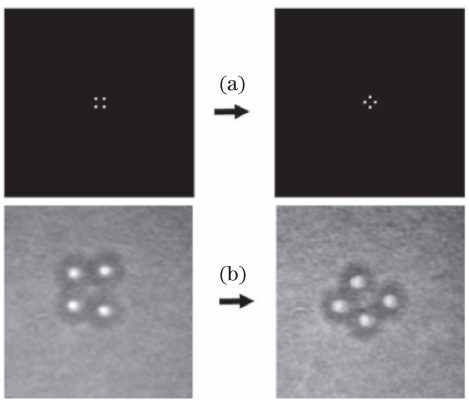

Fig. 7. (a) Object patterns and (b) snapshots of the dynamically trapped particles according to the corresponding optical patterns.

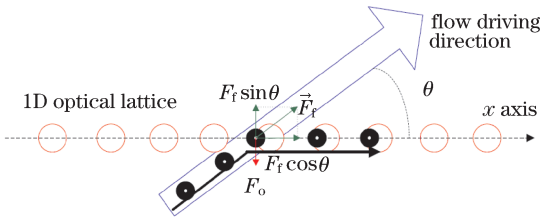

Fig. 8. Trajectories of particles passing through the optical landscape.

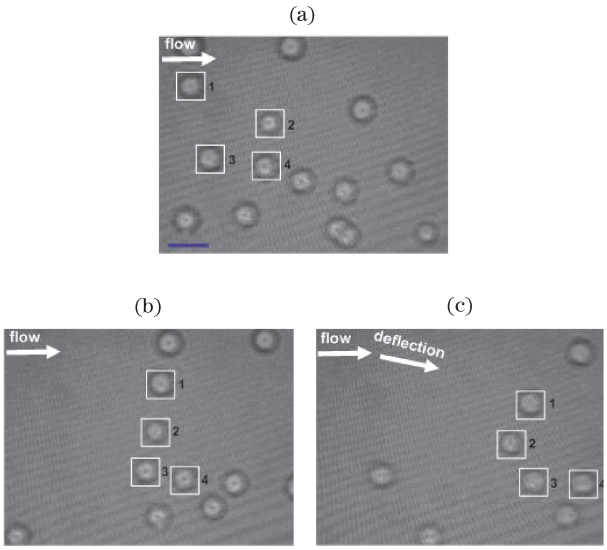

Fig. 9. Locked-in transport of 5-μm silica particles. Scale bar represents 10 μm. Interval is 1 s.

are combined to form a $*$.gif video file, in which the holograms are played repeatedly with intervals of 5 s. When the video is played and the output laser power is 300 mW, the 2×2 array of particles is trapped dynamically following the generated optical patterns by phase hologram. Two representative snapshots of the motion of trapped polymer particles (refractive index $n = 1.59$) with diameters of 3.1 μm are shown in Fig. 7(b).

The theoretical model for optical sorting is briefly illustrated as follows. When a group of particles are passing through an optical energy landscape in microfluidic chamber, two types of forces (optical gradient force and uniform dynamic driving force) are working on the particles. As shown in Fig. 8, the flow driving force is oriented at a fixed angle θ with respect to the potential well of the optical landscape distributed symmetrically about the x-axis. When particles encounter a potential well, their traveling direction may differ from the original driving force direction. The deflection of the particles occurs when the optical force acting on the particle F_o is large enough to balance the y-axis vector of driving force $F_f \sin\theta$. Otherwise, the particles flow along the original driving direction.

The SLM-based optical system was applied to the locked-in transport of silica particles ($n = 1.42$) with identical diameters of 5 μm, sandwiched in the microfluidic chamber with thickness of approximately 70 μm. In Fig. 9, sequential images of the motion of the particles taken with 1-s intervals are shown. With a laser power of 800 mW and a flow speed of 20 μm/s, a strong deflection for the silica particles (highlighted by squares) was observed when they passed through the optical landscape. Evidently, they were deflected and locked into the axis of optical lattice from the top of the image to the bottom. The throughput of the system is approximately 20 particles per second. Figure 9(c) shows the difference between original flow direction and deflection direction.

In conclusion, we adopt the optimized IFTA phase-retrieval GS-AA algorithm for the design of CGH because of its smaller RMSE and more rapid convergence rate. The designed phase hologram is realized through SLM and with the use of holographic microscopic optical system. 2D array of optical spots with good uniformity and relatively high diffraction efficiency of more than 90% is created in the sample plane. Experimentally, we demonstrate dynamic multiple optical trapping with a video combining designed hologram displayed on a computer connected to the SLM. Moreover, continuous locked-in transport of microparticles with the generated optical lattice is experimentally proven.

This work was partially supported by the National Natural Science Foundation of China (No. 60778045) and the Ministry of Science and Technology of China (No. 2009DFA52300) for China-Singapore collaborations.

References

1. A. Ashkin, J. M. Dziedzic, J. E. Bjorkholm, and S. Chu, Opt. Lett. **11,** 288 (1986).
2. K. T. Gahagan and G. A. Swartzlander, Jr., Opt. Lett. **21,** 827 (1996).
3. X. Gan, J. Zhao, S. Liu, and L. Fang, Chin. Opt. Lett. **7,** 1142 (2009).
4. K. Ladavac and D. G. Grier, Opt. Express **12,** 1144 (2004).
5. I. R. Perch-Nielsen, P. J. Rodrigo, and J. Glückstad, Opt. Express **13,** 2852 (2005).
6. M. Zhong, J. Zhou, and Y. Li, Chin. Opt. Lett. **8,** 673 (2010).
7. Z. Ma, K. J. L. Burg, Y. Wei, X.-C. Yuan, X. Peng, and B. Z. Gao, Appl. Phys. Lett. **92,** 213902 (2008).
8. A. Y. Fu, C. Spence, A. Scherer, F. H. Arnold, and S. R. Quake, Nature Biotechnol. **17,** 1109 (1999).
9. E. R. Dufresne and D. G. Grier, Rev. Sci. Instrum. **69,** 1974 (1998).
10. M. P. MacDonald, L. Paterson, W. Sibbett, K. Dholakia, and P. E. Bryant, Opt. Lett. **26,** 863 (2001).
11. R. L. Eriksen, P. C. Mogensen, and J. Glückstad, Opt. Lett. **27,** 267 (2002).
12. C. H. Sow, A. A. Bettiol, Y. Y. G. Lee, F. C. Cheong, C. T. Lim, and F. Watt, Appl. Phys. B **78,** 705 (2004).
13. J. R. Fienup, Opt. Eng. **19,** 297 (1980).
14. R. W. Gerchberg and W. O. Saxton, Optik **35,** 237 (1972).